

HI in the shell elliptical galaxy NGC 3656¹

Marc Balcells², J. H. van Gorkom³, Renzo Sancisi^{4,5}, and Carlos del Burgo^{2,6}

ABSTRACT

Very Large Array¹ (VLA) neutral hydrogen observations of the shell elliptical NGC 3656 reveal an edge-on, warped minor axis gaseous disk ($M_{HI} \sim 2 \times 10^9 M_{\odot}$) extending 7 kpc. HI is also found outside the optical image, on two complexes to the North-East and North-West that seem to trace an outer broken HI disk or ring, or possibly one or two tidal tails. These complexes link with the outer edges of the inner disk, and appear displaced with respect to the two optical tails in the galaxy. The disk kinematics is strongly lopsided, suggesting recent or ongoing accretion.

Integral-field optical fiber spectroscopy at the region of the bright southern shell of NGC 3656 has provided a determination of the stellar velocities of the shell. The shell, at 9 kpc from the center, has traces of HI with velocities bracketing the stellar velocities, providing evidence for a dynamical association of HI and stars at the shell. Within the errors the stars have systemic velocity, suggesting a possible phase wrapping origin for the shell.

We probed a region of $40' \times 40'$ ($480 \text{ kpc} \times 480 \text{ kpc}$) \times 1160 km/s down to an HI mass sensitivity (6σ) of $3 \times 10^7 M_{\odot}$ and detect five dwarf galaxies with HI masses ranging from $2 \times 10^8 M_{\odot}$ to $2 \times 10^9 M_{\odot}$ all within 180 kpc from NGC 3656 and all within the velocity range (450 km s^{-1}) of the HI of NGC 3656. The dwarfs were previously catalogued but none had a known redshift. For the NGC 3656 group to be bound requires a total mass of $3 - 7.4 \times 10^{12} M_{\odot}$, yielding a mass to light ratio from 125 to 300.

The overall HI picture presented by NGC 3656 supports the hypothesis of a disk-disk merger origin, or possibly an ongoing process of multiple merger with nearby dwarfs.

¹Based on observations made with the William Herschel Telescope operated on the island of La Palma by the Isaac Newton Group of Telescopes in the Spanish Observatorio del Roque de los Muchachos of the Instituto de Astrofísica de Canarias.

²Instituto de Astrofísica de Canarias, C/ Vía Láctea, 38200 La Laguna, Canary Islands, Spain

³Department of Astronomy, Columbia University, 550 W. 120th Street, New York, NY 10027, USA

⁴Osservatorio Astronomico di Bologna, Via Ranzani 1, I-40127, Italy

⁵Kapteyn Astronomical Institute, University of Groningen, Postbus 800, 9700 AV Groningen, The Netherlands

⁶Max Planck Institut für Astronomie, Königstuhl 17, D-69117 Heidelberg, Germany

¹The VLA of the National Radio Astronomy Observatory is operated by Associated Universities, Inc. under cooperative agreement with the National Science Foundation.

Subject headings: Galaxies: elliptical and lenticular — galaxies: kinematics and dynamics — galaxies: interactions — galaxies: peculiar — galaxies: individual (NGC 3656, UGC 6400, UGC 6422, MCG +09-19-052, MCG +09-19-056, MCG +09-19-059, MAPS-NGP O_130_0507168)

1. Introduction

NGC 3656 (Arp 155) is a peculiar elliptical galaxy with a nearly spherical body and a dark band running North-South (see Figure 1). A light clump can be seen 45 arcsec South from the center, which is bound to the South by a prominent shell. A number of other, nearly circular shells are seen around the galaxy. The core rotation axis is orthogonal to that of the main body (Balcells & Stanford 1990, hereafter BS90). Two faint optical tails exist around the galaxy (Balcells 1997, hereafter B97). Color maps of the galaxy (B97) show that the shell to the South is distinctly blue ($B - R \approx 0.95$) in relation to the surroundings ($B - R \approx 1.4$), pointing to a young age for its stars. Star formation ($\sim 0.1 M_{\odot} \text{ yr}^{-1}$) is ongoing at the dust lane, as evidenced by extended emission in $\text{H}\alpha$ (B97) and radio continuum (Möllenhoff, Hummel & Bender 1992).

Observations of the 21-cm hydrogen emission line obtained with the Westerbork Synthesis Radio Telescope (WSRT) show that the galaxy contains about $10^9 M_{\odot}$ of neutral hydrogen (Balcells & Sancisi 1996, hereafter BS96). The HI distribution peaks on the dust lane and extends in the North-South direction. The gas on the dust lane shows rapidly rising rotation with velocities reaching up to about 225 km s^{-1} , supporting the hypothesis of a rotating disk seen almost edge-on. In addition to this HI component, there is a central concentration of molecular gas of similar mass (BS96).

NGC 3656 is useful for a study of the origin of gaseous disks in ellipticals because of the large number of peculiarities normally ascribed to interactions that coincide in this galaxy: shells, two tails, peculiar kinematics, peculiar colors, star formation. These can provide constraints on formation scenarios for the gaseous disk. In addition, NGC 3656 is interesting for a study of the HI-shell relation, because of the apparently young dynamical age of the system and because the southern shell is significantly brighter (1.5 mag/arcsec^2) than the galaxy background at that distance from the center.

We present here VLA aperture synthesis HI observations and integral-field spectroscopy (IFS) using fiber optics on NGC 3656. HI measurements are used to describe the gas distribution and velocities with higher resolution and sensitivity than achieved with the WSRT, and to look for the existence of diffuse gas around the galaxy. The IFS of the shell to the south have provided an optical velocity determination for stars associated with the shell.

The optical IFS is presented in § 2. Section 3 describes the HI observations. Results are presented in § 4, for the inner HI disk (§ 4.1), for the extended HI (§ 4.2) and for the shell kinematics (§ 4.3). We discuss the HI results in § 5, the connection between HI and the shell in § 5.1, and

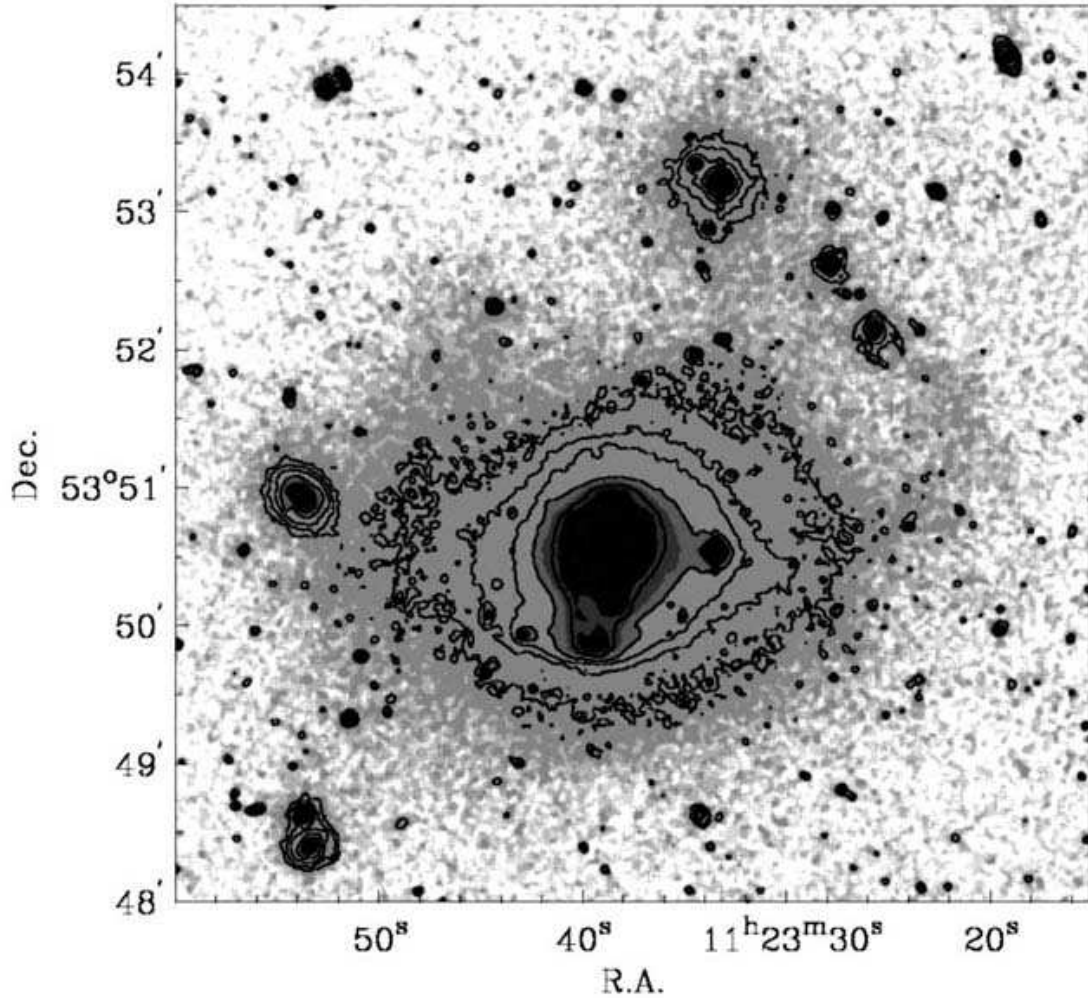


Fig. 1.— R-band image of NGC 3656 (from Fig. 1 of B97). Lowest contour is $26.0 \text{ mag/arcsec}^2$, contour spacing is 0.75 mag . Gray levels, drawn after applying a 5×5 pixel median filter, correspond to $sky - 3\sigma$ (white), $sky - 2\sigma$, $sky - \sigma$, $sky + \sigma$, $sky + 2\sigma$, $sky + 3\sigma$, to show the faintest extended optical structures. Flatfielding of the image is better than 0.2% . Objects at $(\alpha, \delta) = (11:23:33, 53:50:33)$, $(11:23:33.1, 53:53:13)$ and $(11:23:27.7, 53:52:38)$ are stars. Scale is $0.2 \text{ kpc arcsec}^{-1}$.

possible formation scenarios for NGC 3656 in § 5.3. A Hubble constant of $75 \text{ km s}^{-1} \text{ Mpc}^{-1}$ and a distance of 40 Mpc are assumed throughout, giving a scale of $0.2 \text{ kpc arcsec}^{-1}$. All coordinates refer to the J2000.0 equinox.

2. Integral-field optical fiber spectroscopy

We observed the southern shell of NGC 3656 with the William Herschel telescope, on 1998 March 31, using the INTEGRAL fiber bundle system which feeds the WYFFOS Nasmyth spectrograph. For a description of INTEGRAL, see Arribas et al. (1998). We used the SB3 bundle, which contains 135 fibers, each $600 \mu\text{m}$ in diameter (2.7 arcsec on the sky). Of these, 115 densely cover an area of $34'' \times 30''$ on the sky. The distribution of these fibers is hexagonal with a mean distance between them of 3 arcsec . The remaining 20 fibers are set in a ring 45 arcsec in diameter, which is generally used for a sky measurement. We used grating R1200R, which gives a mean dispersion of $1.4 \text{ \AA pixel}^{-1}$ in the spectral range $5640\text{--}7070 \text{ \AA}$ (covering the NaI doublet at 5890 \AA , the 6563 \AA H α line, and the [SII]6716 and 6731 \AA lines). The optical fiber bundle was positioned at $(\alpha, \delta) = (11^{\text{h}}23^{\text{m}}38^{\text{s}}.6, 53^{\circ}49'57''.6)$, $\sim 35 \text{ arcsec}$ south of the galaxy center, and covers from the southern end of the dust lane to beyond the southern end of the shell. The region covered by the bundle is indicated with a thick rectangle in Figure 5.

We followed the data reduction procedure described in del Burgo (2000): bias subtraction, aperture definition and trace, stray light subtraction, extraction of the apertures, wavelength calibration, throughput correction, sky subtraction and cosmic-ray rejection. The throughput correction was done from sky and dome flat exposures. Sky subtraction was accurate to better than 5% rms.

The individual spectra show the NaI absorption doublet and traces of H α , NII and SII emission lines. The weakness of these lines indicates a very slow rate of star formation activity in the shell at present. However, H α absorption indicates that star formation must have been important in the past $\sim 10^9 \text{ yr}$. Overall, the distribution of the H α emission matches the one displayed in the H α narrow-band image in Figure 2b of B97.

We obtained stellar velocities via cross-correlation, using the spectrum of a G2V star as a template. We opted not to use the H α line because, in many fibers, this is partially filled with H α emission. Instead, we used the region around 5890 \AA which includes the NaI doublet. We cross-correlated each fiber spectrum, and excluded those where no convergence was found. We then coadded groups of spectra that showed similar velocities, and cross-correlated these with the template to verify that the results do not depend on the signal-to-noise ratio of the spectra. Because of the intrinsic low signal of each spectrum, the individual fiber velocities have errors around 100 km s^{-1} . Coadded spectra yield velocities with errors around 60 km s^{-1} . The errors are probably conservative as cross-correlation is known to overestimate velocity errors (BS90; Jedrzejewski & Schechter 1988). This yielded three velocity values centered at positions 25, 33 and 41 arcsec South

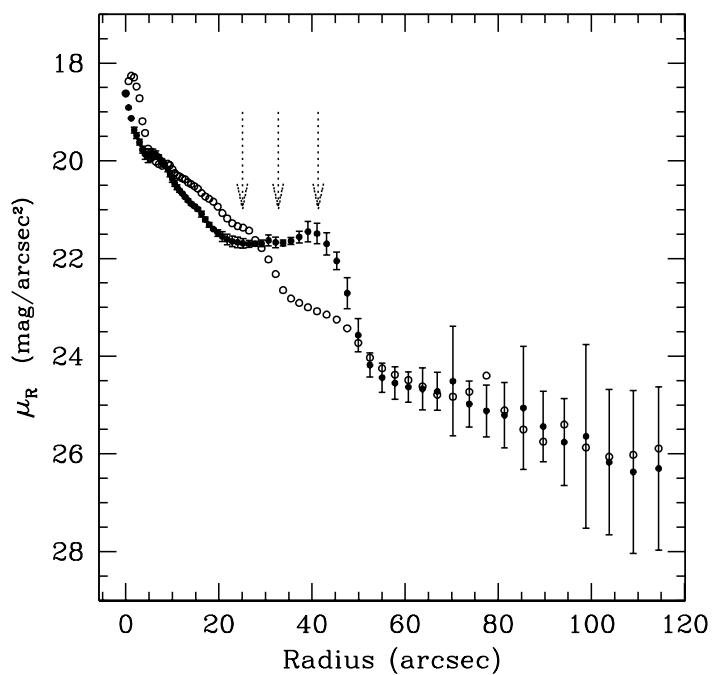


Fig. 2.— R-band surface brightness profiles of NGC 3656 on 25°-wide wedge-shaped apertures centered on the galaxy nucleus, along PA=170° (filled symbols, with error bars) and along PA=10° (open symbols, error bars omitted). Vertical arrows indicate the central positions of the apertures where optical velocities from 2D fiber spectroscopy are measured.

from the center. These synthesized apertures are indicated with rectangles in Figure 5.

To show the three optical velocity apertures with respect to the southern shell, we plot R -band surface brightness profiles along wedge-shaped apertures along PA=170° and PA=10°, centered on the galaxy nucleus (Figure 2). The vertical arrows locate the center positions of the three fiber velocity data apertures. We take the North profile as an estimate of the underlying galaxian surface brightness distribution, and use this to measure the surface brightness contrast at the South shell. The latter, at $R = 45$ arcsec, has $\mu_R = 21.5$ mag/arcsec⁻², 1.5 mag arcsec⁻² brighter than the background. The outermost velocity point is centered on the South shell, thus the measurement traces the shell velocity with little background contamination. At the locations of the two innermost measurements the surface North and South surface brightness are comparable, suggesting that these two measurements trace the underlying galaxy velocity field. Optical velocity results are presented in § 4.3.

3. HI observations

Neutral hydrogen VLA observations were made in D array (1 km) in september 1996. The VLA data confirmed the presence of HI associated with the dust lane and southern shell inferred in the WSRT data, and also reveal the presence of low surface brightness extended HI around the galaxy. The HI emission at anomalous velocities in the south shell region (Fig. 2 of BS96) was not confirmed. The data looked complex enough for a proper multi configuration study to allow the gas to be compared with optical structures on all scales. Here we present the combined results of 4 hours of D, 8 hours of C and 16 hours of B configuration, data taken in September 1996, September 1997 and February 1997, respectively. For all observations a total bandwidth of 6.25 MHz was used, centered at 2870 km/s. The correlator was used in 2 IF mode with no online Hanning smoothing. This produced 63 channels, with 21 km s⁻¹ channel separation. Useable data were obtained over the velocity range from 2365 km s⁻¹ to 3521 km s⁻¹. Standard VLA calibration procedures were used, initially separate data cubes were made for each of the configurations to inspect the data. Then the continuum was subtracted in the UV plane by making a linear fit through the line free channels. The UV data were then combined and image cubes were made with various weighting schemes. Here we present the results of the full resolution data, using uniform weight and robust 1, giving an angular resolution of 7.3x7.2 arcsec and an rms noise of 0.16 mJy/beam (1 mJy/beam = 11.4 K) and images made of the C and D array only, with a resolution of 25.2x19.7 arcsec and an rms noise of 0.23 mJy/beam (1 mJy/beam = 1.21 K). This translates into typical column density sensitivities (2σ) of 1.4×10^{20} cm⁻² in the BCD array and 2×10^{19} cm⁻² in the CD array. Our $6\text{-}\sigma$ HI mass limit over 40 km s⁻¹ is $2 \times 10^7 M_\odot$ in the center of the field.

Table 1. HI data for NGC 3656 and detected companions

| Name | RA (2000) | Dec (2000) | V_{HI} km s ⁻¹ | $\Delta(V_{HI})^a$ km s ⁻¹ | M_{HI}^b Jy km s ⁻¹ | $10^9 M_{\odot}$ |
|------------------------|------------|------------|--------------------------------|--|-------------------------------------|------------------|
| NGC 3656 | 11 23 38.4 | 53 50 30 | 2870 | 425 | 5.40 | 2.0 |
| MAPS-NGP O_130_0507168 | 11 22 23.6 | 53 51 54 | 3059 | 105 | 0.47 | 0.18 |
| MCG +09-19-052 | 11 22 25.2 | 53 41 17 | 2944 | 168 | 3.40 | 1.3 |
| MCG +09-19-056 | 11 23 02.5 | 53 41 47 | 2796 | 168 | 4.99 | 1.9 |
| MCG +09-19-059 | 11 23 16.0 | 53 47 14 | 2796 | 126 | 0.78 | 0.29 |
| UGC 6422 | 11 24 44.7 | 53 44 36 | 2996 | 126 | 0.45 | 0.17 |

^aFull velocity range over which HI is detected.

^bHI mass uncertainties are approximately 10%.

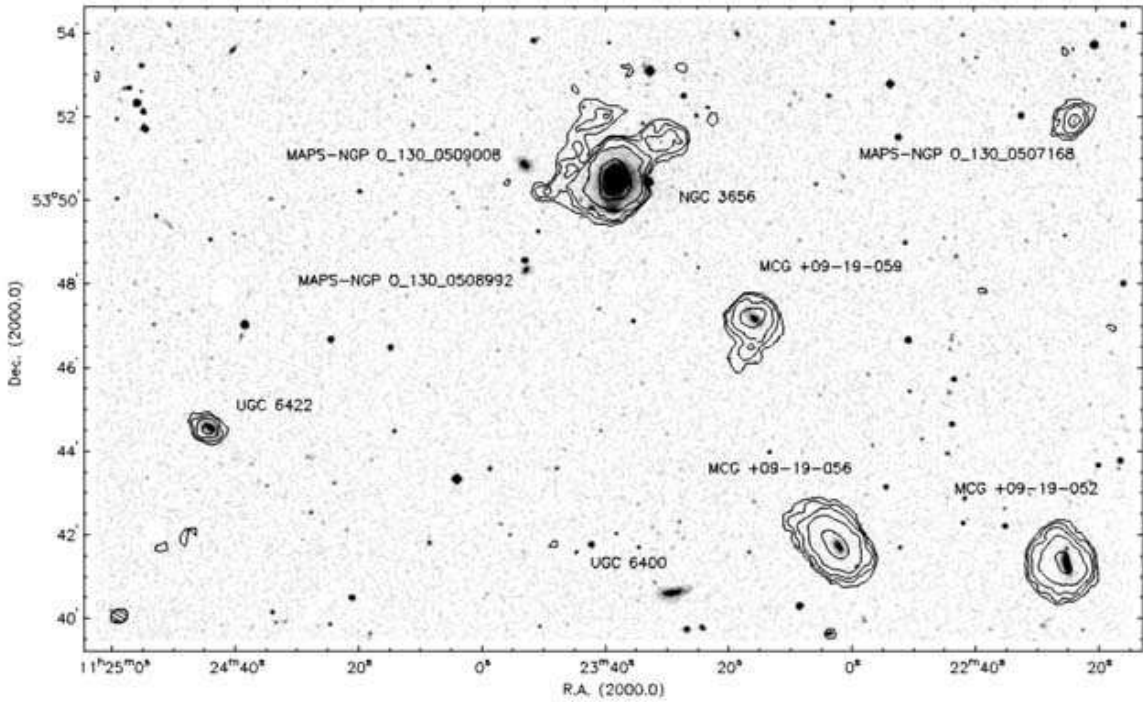


Fig. 3.— Total HI contours from the C and D array data (25 arcsec resolution) overlaid on a DSS image. Field size is $25' \times 15'$. HI contours are 0.23, 0.57, 1.1, 2.3, 6.8, 11.4, 16.0 $\times 10^{20}$ cm⁻².

4. Results

HI associated with NGC 3656 is detected over the range of 2600 to 3100 km s^{-1} , with an integrated HI flux of $5.4 \pm 0.4 \text{ Jy km s}^{-1}$, in good agreement with the single-dish value of $5.3 \pm 1 \text{ Jy km s}^{-1}$ obtained at Jodrell Bank (BS96). In addition five small spirals and dwarf irregulars are detected within the velocity range of NGC 3656, all within $\sim 180 \text{ kpc}$ of NGC 3656. Figure 3 shows the total HI distributions for the six detected galaxies over a Digitized Sky Survey image. None of the companions had a previously measured redshift. The parameters of these galaxies are listed in Table 1. Together, the observations indicate that NGC 3656 is in an HI rich environment.

MGC +09-19-059, at 24 kpc to the south-west of NGC 3656, shows an outer HI extension toward the south. At very low levels ($1\text{-}\sigma$) there is evidence for a bridge between MGC +09-19-056 and MGC +09-19-059 at 2744 km s^{-1} , and at even lower levels there may be a connection between MGC +09-19-059 and NGC 3656 at 2807 km/s .

The HI density distribution of NGC3656 shows a North-South disk seen almost edge-on which coincides in the inner part with the dust band, and extensions on a larger scale surrounding the optical picture. At the galaxy center there is a radio continuum source slightly extended North-South and coinciding with the dust lane. It has a peak of 10 mJy/beam and total flux density of $24 \pm 1 \text{ mJy}$. This source had been reported by Möllenhoff, Hummel & Bender (1992).

4.1. The inner HI disk

The distribution and kinematics of the gas at the highest angular resolution of 7 arcsec is displayed in the channel maps of Figure 4. The high resolution total HI map (Fig. 5) shows a concentration of HI running North-South in the inner parts and well aligned with the dust lane. This forms an inner disk seen nearly edge-on. The central, innermost contour encircles a local minimum due to absorption against the central radio continuum source. Further out the disk seems to become warped, oriented more North-West/South-East and apparently more face-on. The kinematic structure of the edge-on disk is shown in the position-velocity map at position angle 170° (Fig. 6). This is in the direction from the center to the southern optical shell. The pattern of rotation is clear, with the southern side receding and the northern approaching and a steep rise in the rotation curve near the center. The velocity range is from about 2650 to 3100 km s^{-1} , corresponding to 225 km s^{-1} maximum rotational velocity, and the mid-point velocity is approximately 2875 km s^{-1} , in good agreement with the optically determined stellar systemic velocity ($2869 \pm 13 \text{ km s}^{-1}$, BS89). The warped disk extends to 35 arcsec (7 kpc) from the center.

The disk kinematics is strongly lopsided. While inside 10 arcsec of the center, where the maximum rotational velocity of 225 km s^{-1} is reached, the rotation pattern is symmetric, beyond 10 arcsec the rotational velocities remain constant on the northern side whereas they drop by a factor of 2 ($\sim 100 \text{ km s}^{-1}$) on the southern side. This asymmetric velocity structure indicates large

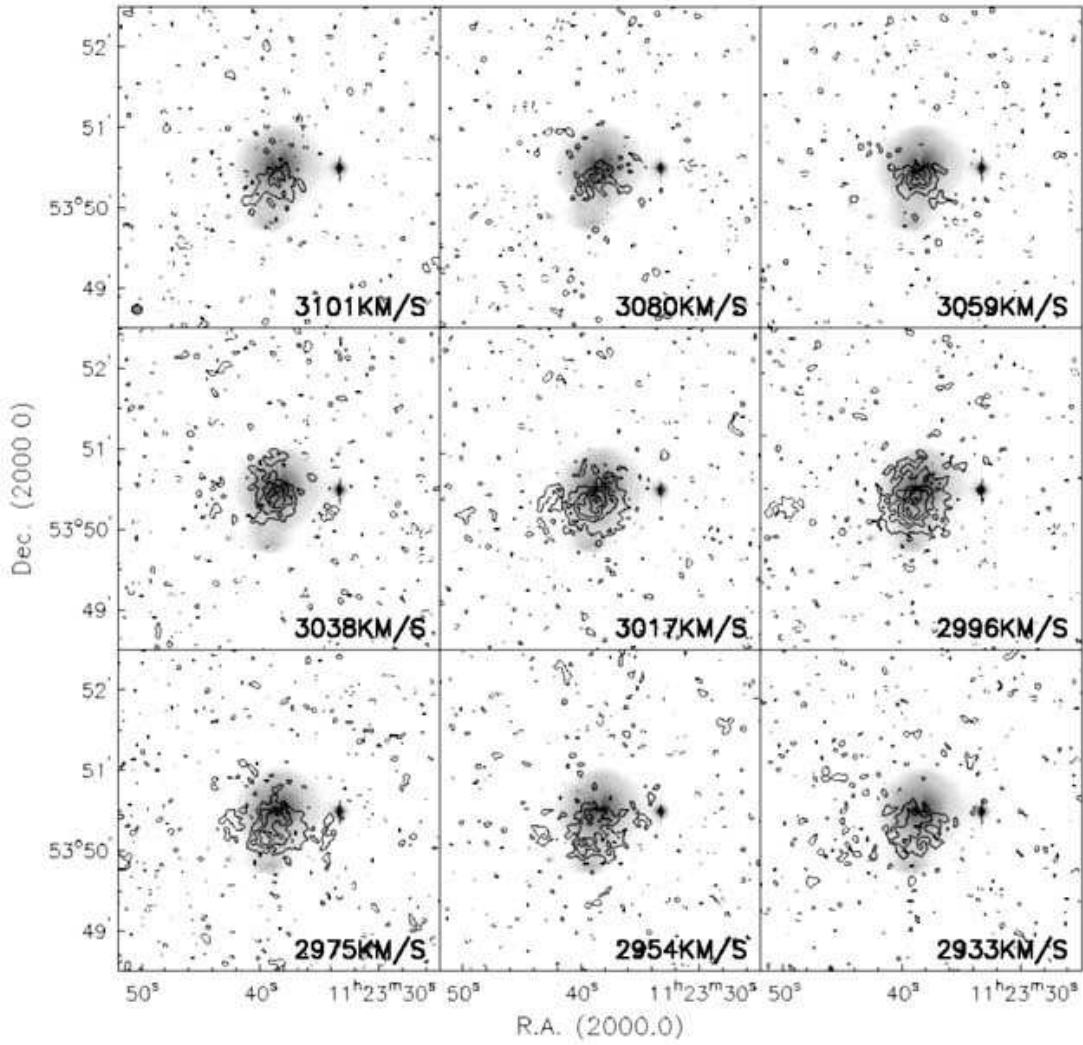


Fig. 4.— Channel maps for the data cube derived from BCD array data. Grayscale is the R band image. Contours are -0.64, -0.32 (dashed), 0.32, 0.64, 0.96, 1.128, 1.60 mJy/beam. Beam is $7.3'' \times 7.2''$. Noise is 0.16 mJy/beam rms.

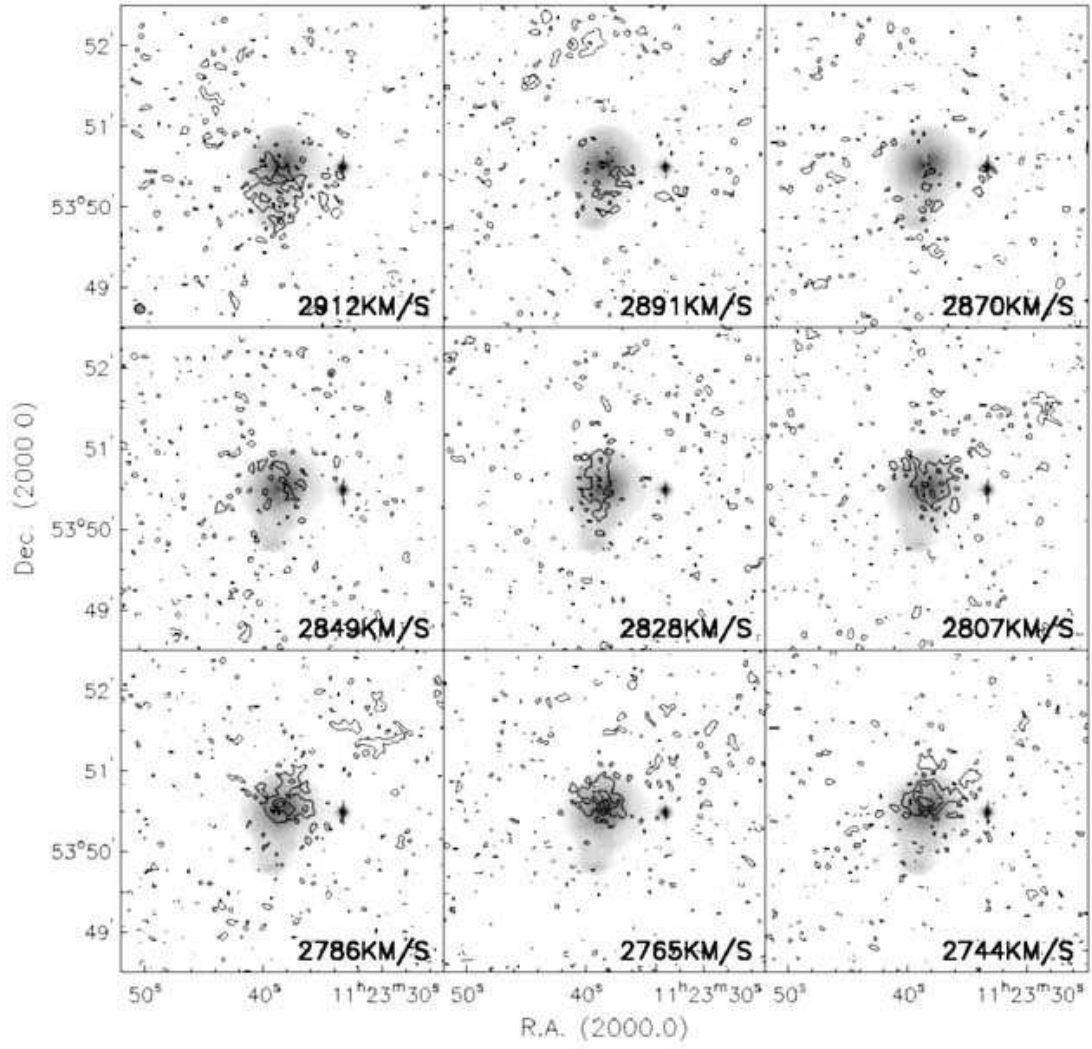


Fig. 4.— Continued.

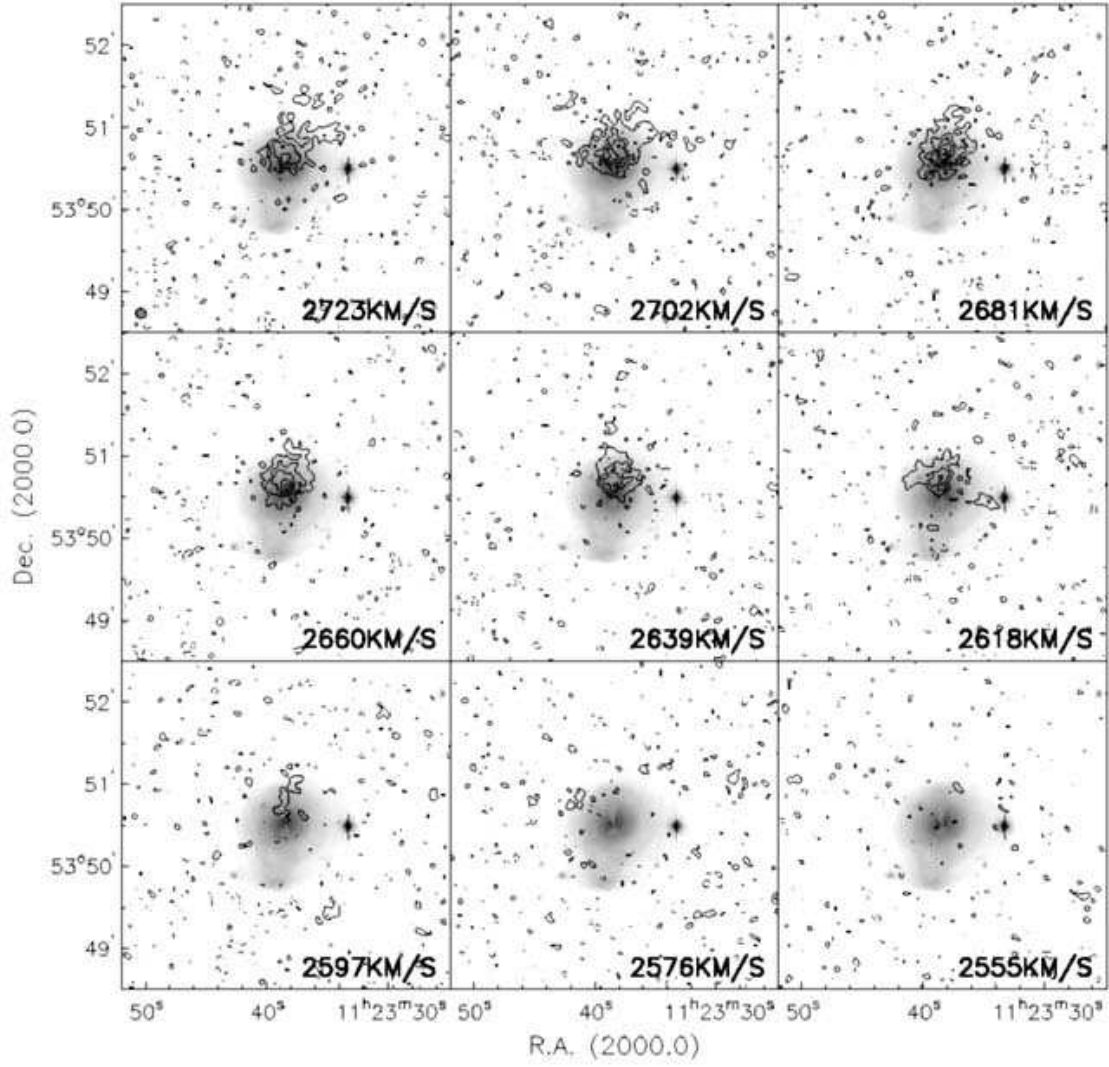


Fig. 4.— Continued.

NGC 3656 . Contours=totHI 7" . Colour=R .

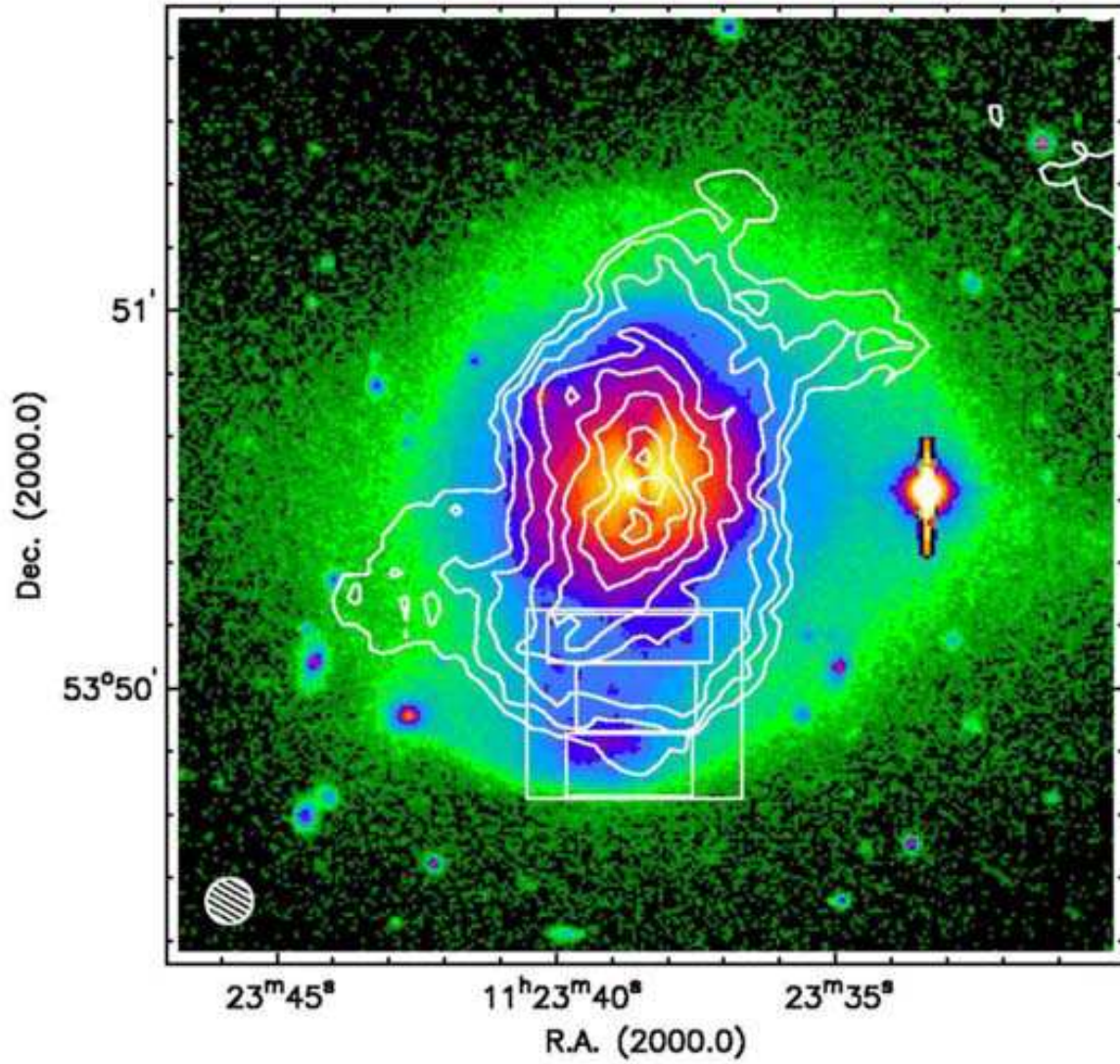


Fig. 5.— Contours of total HI flux from BCD array data. Beam is 7" FWHM. HI contours are 2.1, 5.2, 10, 21, 31, 42, 52, 62 $\times 10^{20} \text{ cm}^{-2}$. *Thick box*: Aperture of the 2D fiber bundle spectrograph. *Thin boxes*: Synthetic apertures for stellar velocities derived from the 2D optical fiber spectroscopy.

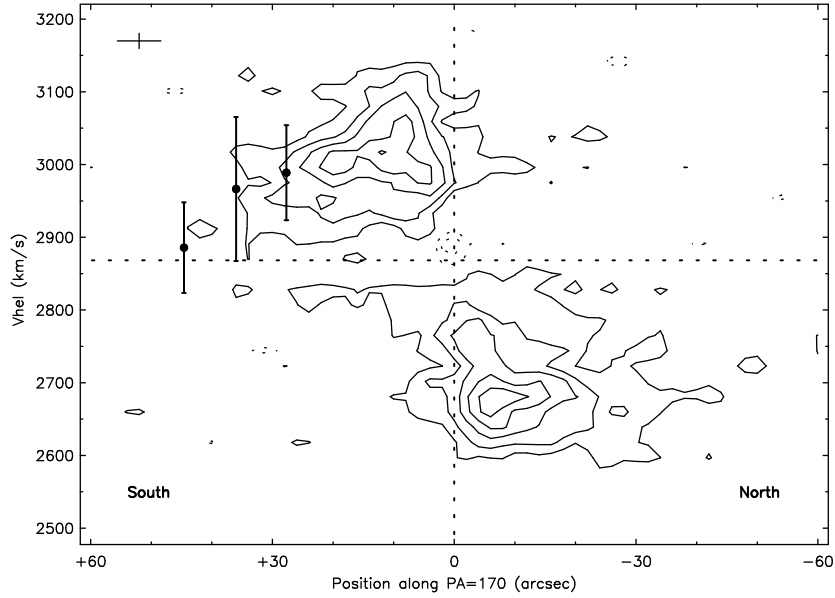


Fig. 6.— *Contours*: Position-velocity diagram along position angle 170° , centered on the nucleus of NGC 3656. The origin is set at the position of the radio continuum source. The horizontal dotted line indicates the optically-determined systemic velocity (2969 km s^{-1}). The cross indicates the spatial resolution ($7''$) and velocity resolution (21 km s^{-1}). Contours are $-0.96, -0.64, -0.32$ (dotted), 0.32 ($2\text{-}\sigma$), $0.64, 0.96, 1.128, 1.60 \text{ mJy/beam}$. *Points*: NaI $\lambda 5890$ optical stellar velocities derived from 2D optical fiber spectroscopy near the southern shell. Note the absorption at slightly redshifted velocity.

deviations from circular motion – possibly gas on eccentric orbits suggesting a young dynamical age for the disk. Non-circular motions may contribute to the important velocity broadening toward systemic velocity visible on both sides of the galaxy. On the southern side, low velocity gas (2912 km s^{-1} , 35 km s^{-1} above systemic) is seen at all radii. There are traces of emission at apparently counterrotating velocities, approaching in the southern (2800 km s^{-1}) and receding in the northern quadrant. These may partly be explained by the outer warp geometry. They may also trace HI in highly elongated orbits associated with the southern shell (see § 4.3).

The effect of absorption against the central radio continuum source is clearly shown by the hole near the systemic velocity in the position-velocity map (Fig. 6), as expected in an edge-on disk. The absorption is also present at velocities higher than the systemic velocity (-0.74 mJy at 2891 km s^{-1} and -0.45 mJy at 2870 km s^{-1} .) This provides evidence for non-circular motions.

To investigate the relation of the HI and the shell, we plot in Figure 7 a Renzogram (Schiminovich, van Gorkom, & van der Hulst 2001): one contour (0.64 mJy/beam , $3\text{-}\sigma$) from each channel map, with color-coded velocity, is plotted on top of a gray-scale *R*-band image. This figure may be used to analyze the relation between the rotating system of HI and the southern shell. HI is detected at the shell in the 2912 km s^{-1} channel only. The channel maps in Figure 4 also show that the HI only reaches the shell in this channel, at the $4\text{-}\sigma$ level, with traces of HI beyond the shell in the 2870 km s^{-1} channel. The other velocity channels do not quite reach the shell at the $3\text{-}\sigma$ level. Most velocity contours pile up at ~ 35 arcsec from the center. Therefore, despite its proximity, the shell does not appear to lie within the main HI rotating system, but is slightly offset to the outside of it. We find measurable HI on the shell, which does not rotate with the main HI disk but, rather, displays a narrow range of near-systemic velocities.

The strong velocity broadening in the disk is apparent in the superposition of the velocity contours, as is the warp geometry. The color coding shows that the intermediate velocities at the North and South tips of the disk link smoothly with the extended HI emission further out.

4.2. Extended emission

The C and D array data reveal HI emission further out than the ~ 35 arcsec radius of the main disk. The most striking characteristic of the extended emission is its strongly asymmetric distribution with respect to the optical galaxy. The total HI 25 arcsec resolution map is shown in Figure 8, overlaid on a high-contrast optical image. While on the southern side the HI distribution ends rather sharply at the radius of the main disk, two HI complexes extend to the north. One starts at the south-eastern side of the inner HI system and extends like a long arm ($130 \text{ arcsec} = 26 \text{ kpc}$) towards the North. Its velocity (Fig. 4) declines smoothly from about 2933 km s^{-1} in the East to 2891 km s^{-1} in its northern tip. Another feature starts at the North end of the inner disk and extends in the North-West direction. Its velocity increases from 2723 km s^{-1} at its base to 2807 km s^{-1} at its tip. These two complexes may be tidal tails, given the asymmetry to the north

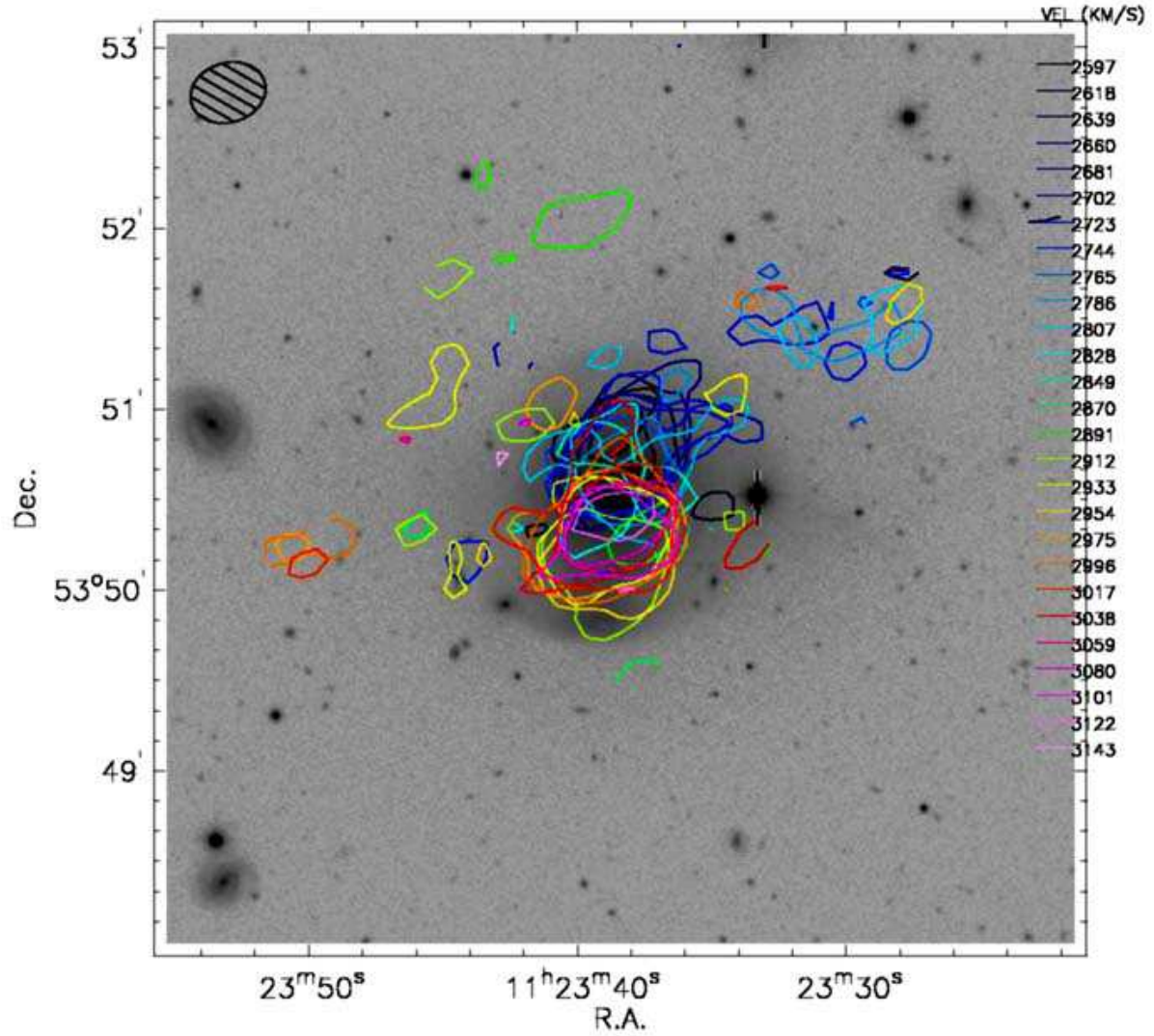


Fig. 7.— Contours of flux density 0.64 mJy/beam in the CD data cube, overlaid on an R-band image of NGC 3656. Velocities corresponding to each color are given in the legend. A mask was applied to each channel, built from a Gaussian-smoothed total HI map, in order to highlight the velocity structure of the extended components. Beam size is $25.2'' \times 19.7''$. Noise is 0.23 mJy/beam rms.

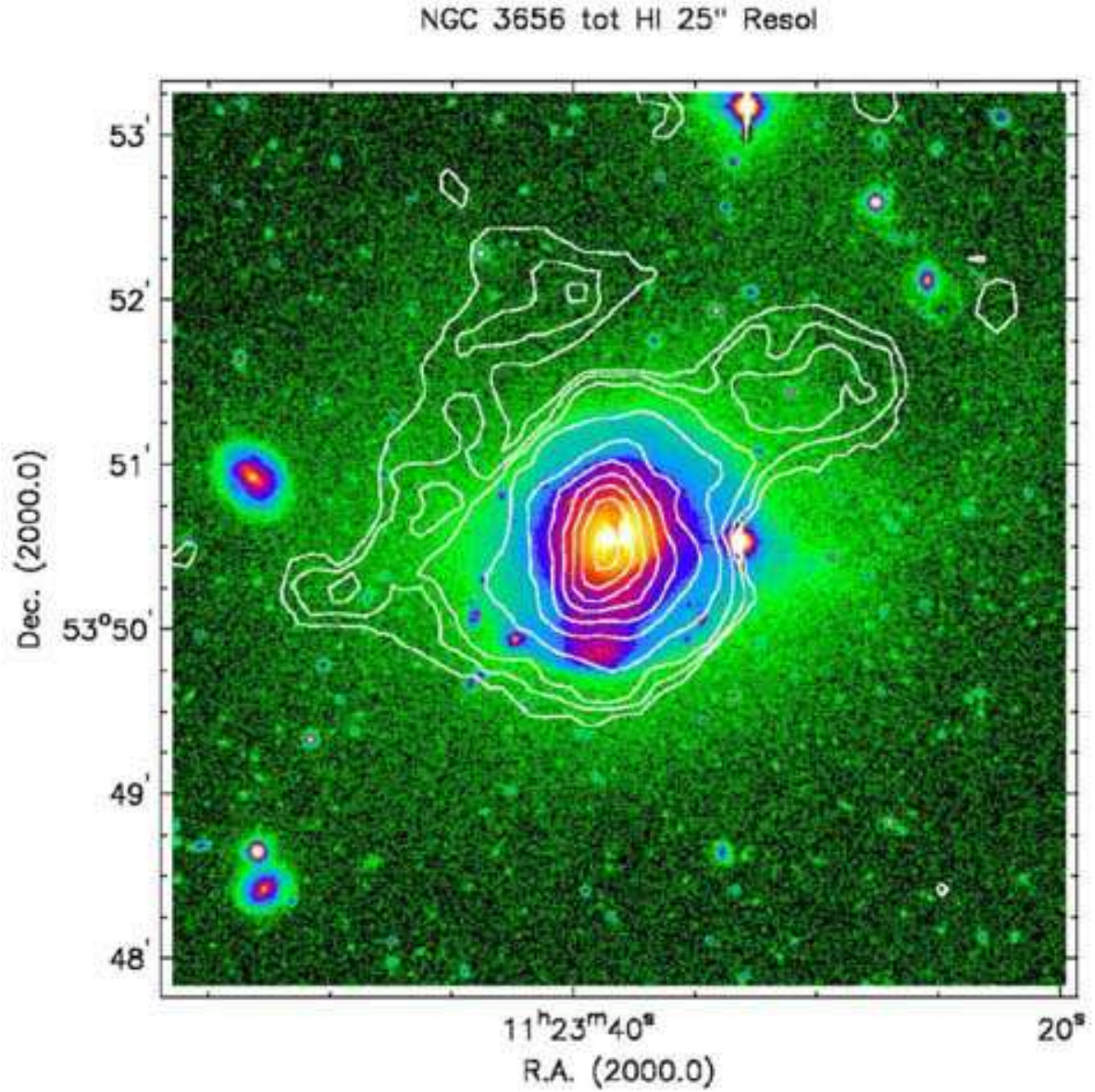


Fig. 8.— Contours of total HI flux from the CD array data. Beam is $25.2'' \times 19.7''$. HI contours are 0.23, 0.57, 1.1, 2.3, 4.6, 6.8, 9.1, 11.4, 13.7, $16.0 \times 10^{20} \text{ cm}^{-2}$. *Grayscale*: R-band image of NGC 3656, with gray scale stretched to show the faintest extended structures.

of the extended distribution and the smooth velocity profiles along the features. An alternative possibility is that they may form part of an outlying, broken, extended and warped disk or ring. The observed velocities may then be understood as due to the more face-on view of the outer gas as well as to non-circular motions. These features connect with the warped gaseous disk in the main body of the galaxy. The total HI mass of these two complexes is $1.9 \times 10^8 M_{\odot}$, roughly 9% of the total HI detected in the system. The eastern HI feature is parallel but slightly offset inward with respect to the eastern optical tail reported by B97, which is shown in Figure 8. The North-West HI feature has no apparent optical counterpart; the western optical tail curves around the HI (Fig. 8). Such anti-correlation of HI and optical tails has been found in other merger remnants, eg. NGC 520 (Hibbard & van Gorkom 1996) and NGC 2865 (Schiminovich et al. 1995). See Hibbard, Vacca, & Yun (2000) and Mihos (2001) for possible explanations of these morphologies.

4.3. Shell kinematics

Stellar velocities derived from the integral-field optical fiber spectroscopy (§ 2) are shown in Figure 6 overplotted on the HI position-velocity diagram. The two innermost points lie within the rotating system described in § 4.1, and their velocities match those of the HI. These measurements trace the general stellar velocity field rather than the clump/shell velocity (§ 2). Thus, stars near the galaxy’s minor axis rotate with the HI. The stars could have been accreted with the HI, or may have formed in place out of the HI disk. The pronounced blue colors in this region ($B - R \sim 0.9$, B97) and the traces of $H\alpha$ absorption (§ 2) indicate a young age, and the disk is actively forming stars further in, out to 3 kpc from the center (BS96).

At the outermost point the mean velocity is $2886 \pm 61 \text{ km s}^{-1}$. This point is centered on the bright clump (see Fig. 2), and thus provides velocity information closest to the southern shell. It is interesting that the velocity at this point lies quite close to the galaxian systemic velocity ($2869 \pm 13 \text{ km s}^{-1}$). The error bar of the shell velocity, which gives the rms scatter of the individual fiber velocities, constraints the l.o.s. velocity to less than 30% of the galaxy circular velocity, which from the overall HI rotation curve we estimate as $V_{circ} \approx 200 \text{ km s}^{-1}$ at the galactocentric distance of the shell. Even accounting for a comparable velocity component perpendicular to the l.o.s., the orbits must be fairly elongated. Trial N-body experiments indicate that, if the shell material is at apocenter with tangential velocity below 30 % of the circular velocity, the orbit eccentricity is above 0.8 and the pericenter distance is below $0.3R_{eff}$. Such radial orbit for the clump suggests that the shell results from the piling up of stars at the apocenters of their orbits, rather than from the bending of a sheet of stars in near-circular orbit seen edge-on at its tangential point. I.e., while the stars cannot be constrained to a strictly radial orbit, the shell appears to be more a result of phase-wrapping (Quinn 1984), than space-wrapping (Dupraz & Combes 1987, Hernquist & Quinn 1987).

At the location of the clump in the shell, HI is detected at 2912 km s^{-1} , plus traces further out than the shell at 2870 km s^{-1} (Figs. 4, 7). These velocities bracket the optical velocity of the shell.

The strong detection at 2912 km s^{-1} (above 4σ) indicates that the HI at the shell is dominantly at velocities that match the shell stellar velocity, and provides kinematic evidence that the HI and the stars are dynamically associated at the shell.

5. Discussion

The elliptical galaxy NGC 3656 has remarkable optical and HI properties. The optical picture is already complex, with a minor axis dust disk harboring an extended starburst, a North-South blue ring, two optical tails, a prominent shell, a number of other faint shells (BS90, B97). The HI data presented here adds to the complexity, showing a minor axis warped gaseous disk and two gaseous complexes or tails extending to the North of the galaxy. The HI distribution is asymmetric in two respects: there is a strong positional asymmetry in the external gas, and a strong kinematic asymmetry in the HI disk inside the galaxy. Neutral hydrogen appears to be dynamically associated to the shell to the South of the main body.

Main questions on the HI disk structure are the pronounced broadening of the position-velocity distribution toward systemic velocity and the strong velocity lopsidedness (Fig. 6). Modeling will be needed to determine the relative importance of the warp, the disk internal velocity dispersion and line-of-sight integration effects on the velocity broadening. Modeling may clarify as well if elliptical orbits in the disk or associated with the shell are required to explain the velocity lopsidedness.

It is likely that the asymmetry in the HI velocity distribution is also related to accretion from the external complexes, with HI dominantly falling from the North causing the observed kinematic asymmetries. That accretion is taking place may be inferred from the geometry of the east complex: for this system to wrap around the galaxy, from its base on the South to its North tip, it needs to be on the near side to the observer, otherwise its angular momentum would be opposite to that of the gas disk. The velocities above systemic then indicate that the gas in the complex is falling onto the galaxy.

An order-of-magnitude estimate of the gas accretion rate may be derived from the masses and velocities of the external complexes. For the North-East arm, the rate is $\sim 0.2 M_{\odot}/\text{yr}$. At this rate, both systems would take 5 Gyr to deliver the gas currently present inside NGC 3656. Accretion is likely to have been more efficient in the past, hence the age of the event that originated the accretion is likely to be much shorter. If the rate continues as it is now, NGC 3656 will continue to accrete gas for at least another ~ 0.5 Gyr, probably longer if the tips of the arms are on less bound orbits.

That the external complexes trace tidal tails rather than an external disk or ring remains open to interpretation, as is the case for the extended HI distributions in other merger remnants (NGC 520, Hibbard & van Gorkom 1996; NGC 5128, Schiminovich et al. 1994). Tails and inclined rings may have similar kinematic signatures when seen in projection, despite tails being on fairly elongated orbits. In NGC 3656, the strong lopsidedness of the external HI together with the

kinematic peculiarities in the inner disk favor the tail interpretation. But it is unclear whether the extended material, or part of it, describes an extension of the inner warped disk. In either interpretation, the long dynamical times in the outer parts make it unclear what the evolution of the gas and stars might be when the merger signatures in the inner parts fade out. Some of this material may evolve into the type of HI-delineated outer shells seen in eg. NGC 5128 and NGC 2865 (Schiminovich et al. 1994, 1995) – see in particular the channel maps at 2912 and 2891 km s^{-1} .

As the system evolves, the disk should grow in radius as the high angular momentum material at high radii settles into organized orbits. This should happen in about 1 Gyr, roughly the orbital period at the tip of the extended complexes at 26 kpc.

5.1. Shell dynamics

The first detection of HI near the shells in NGC 5128 (Schiminovich et al. 1994) brought the question of whether gas and shell stars are dynamically associated or simply projected along the line of sight (van Gorkom & Schiminovich 1997). Our measurements provide evidence that the shell stars and the HI in NGC 3656 share a similar line-of-sight velocity and hence are most likely dynamically associated.

To our knowledge the southern shell in NGC 3656 is the first shell for which stellar velocity information becomes available. Our results show that IFS provides a means for obtaining velocity information of shells and other extended, low-surface brightness objects by co-adding over two-dimensional apertures. Our formal errors are large, highlighting the difficulty of the measurement, and deeper data will be valuable to confirm the results. We attempted this measurement on NGC 3656 because the southern shell is significantly brighter than most shells in other galaxies. However, in NGC 3656 the measurement is made difficult by weak line strengths due to low metallicity and/or dilution by a young stellar continuum throughout this galaxy (see the spectrophotometric data on NGC 3656 in Liu & Kennicutt 1995). IFS measurements of shell stellar kinematics may be successful on massive ellipticals with red shells, even if fainter than the shell observed here.

Our measurement highlights the possibility to sort out the phase-wrapping vs. space-wrapping dichotomy for shells on the basis of data. To date dynamical models for shells have had to rely on morphological information only to constrain the types of orbits of the shell material.

It was unexpected to us that the NGC 3656 shell should be on a phase-wrapping orbit. There is little evidence for shell interleaving in this type-2 (Prieur 1990) shell system. Given the shell’s proximity to the disk of HI, we suspected a low- to moderate-ellipticity orbit for the shell material, hence a space-wrapping nature for the shell. In the similar galaxy NGC 5128, the high angular momentum of the stellar halo traced by planetary nebulae (Hui et al. 1995) and the high rotation velocity of the HI near the shells together point to high-angular momentum shells (Schiminovich

et al. 1995). To explain the nearly radial orbit of the shell of NGC 3656, one possibility is that disruption near pericenter and dynamical friction remove angular momentum from the collisionless component of the merging object, so that stars and gas decouple from each other. Gas and stars should be expected to follow different dynamics during the merger anyway for the gas to form an ordered disk.

Neutral gas in shells has been seen as a problem for the phase-wrapping mechanism. SPH modeling (Weil & Hernquist 1993) shows that gas-rich shells in radial orbits get easily stripped of their HI as shells cross paths. The main shell in NGC 3656 has apparently managed to keep some of its HI. Stripping efficiency may be reduced if the gas at the shell, and/or in the disk, is distributed in discrete clouds; the fate of gas in shells varies significantly depending on whether the gas is modeled as a continuous medium or as discrete clouds (Kojima & Noguchi 1997, Combes and Charmandaris 1999). The frequency of gas cloud collisions with the disk may be further reduced if the disk is geometrically thin.

5.2. The shell unusual brightness

The southern shell of NGC 3656 is atypical for its high surface brightness ($1.5 \text{ mag}_R \text{ arcsec}^{-2}$ over the background, Fig. 2). Its integrated magnitude, after subtracting a smooth elliptical model of NGC 3656, is about $R = 15$, about 5% of the total R -band light of the galaxy. While its blue colors indicate young stars, the shell appears also in K -band images, hence its high surface brightness cannot entirely be ascribed to young stellar populations. Taking into account $B - R \sim 1.0$ (B97), the shell has an absolute magnitude $M_B \sim 17$ comparable to that of a typical dwarf galaxy. This shell is thus produced by a fairly massive component. The pronounced surface brightness drop beyond the shell indicates that few stars at the shell location presently have orbital energies higher than those of the shell. Such order is hard to maintain after a pericenter passage near the galaxy center. These characteristics may probably be explained with a young age for the shell. The shell material still retains a memory of its initial orbit at present. Phase wrapping after several orbits might dilute the present shell into an ensemble of fainter shells with brightness comparable to those typically found in ellipticals.

With $\sim 5\%$ of the total galaxy light, presently the shell tidal field might influence the dynamics of the HI disk, perhaps contributing to its kinematic lopsidedness. N-body modeling should allow to test this hypothesis.

5.3. Formation scenarios

NGC 3656 stands out among peculiar ellipticals for the number of features related to merger and accretion processes occurring simultaneously in the same object. What is the origin of so many peculiarities?

B97 proposes that NGC 3656 formed in a major merger of two spirals, given the presence of two optical tails. This merger should have formed the entire elliptical galaxy, including its system of shells, and have dumped the observed neutral gas. In merger simulations, the gaseous components of the precursor galaxies form centrally concentrated disks while 5–50% of the gas is ejected into extended tidal components (Barnes & Hernquist 1996, Barnes 2001), a picture that matches the HI distribution of NGC 3656. Spiral-spiral mergers produce polar gaseous rings under certain orbital configurations (Bekki 1998).

Shell formation in major mergers was modeled with N body techniques by Hernquist & Spergel (1996). In their scenario, shells form out of returning tidal material. In NGC 3656, that the brightest shell lies at the base of one of the tidal tails and near the HI disk provides support for a connection of the shell to the gas accretion. That such subsystem would have a sharp edge may be caused by the narrow ranges of orbital energy and angular momentum of the HI returning to the galaxy along the tidal tails. The blue colors in the shell also support the connection between the shell and the gas accretion. The lack of H α emission, indicating the absence of early B-type stars, places a lower limit to the age of the shell stars at $\sim 10^7$ yr (eg. Leitherer et al. 1999), while the presence of H α in absorption places a less-well defined upper limit at ~ 1.5 Gyr. The galaxy’s crossing time at the shell radius is 0.6 Gyr. Hence, the spectral signatures at the shell indicate ages that are typical of advanced merger remnants, ie a few remnant’s crossing times. Note that these ages are consistent with some of the stars being born in place after the accretion event, perhaps by compression of the gas clouds in their passage through the inner galaxy. The role of star formation in building shell systems has been largely unexplored, and could be relevant to explaining the puzzling color properties of shells (Prieur 1990).

Overall, the major-merger hypothesis provides a consistent picture for the formation of the merger signatures of NGC 3656 in a single process. Other interpretations are also plausible, in which different processes account for the various peculiarities. The blue colors of the shell ($B - R \sim 1.0$, B97) correspond to those of a late-type, low-metallicity galaxy, and thus could trace the ingestion of a satellite by NGC 3656. Several gas-rich galaxies exist in the vicinity of the galaxy, with sufficient gas to provide the $\sim 10^9 M_{\odot}$ of HI present in the NGC 3656, while the accretion of other satellites could have produced the optical tidal tails and the shells. The presence of several gas rich companions to HI-rich ellipticals is common. For the NGC 3656 group to be bound, using the mass estimators of Heisler et al. (1985), we require from $3 \times 10^{12} M_{\odot}$ to $7.4 \times 10^{12} M_{\odot}$, yielding mass-to-light ratios $(M/L)_B$ from 125 to 300 in Solar units (adding the light of all galaxies within 200 kpc and using our own photometry of NGC 3656, the dominant contributor). The halo mass is typical for L_{\star} galaxies (Zaritsky et al. 1997), suggesting that the NGC 3656 group may indeed be bound. NGC 3656 may represent a case of a multiple accretion onto an existing elliptical. Such process may continue in the future with the accretion of the five galaxies that lie within 180 kpc of NGC 3656, representing the collapse of a loose group leading to the formation of a massive field elliptical.

NGC 3656 shares striking similarities with the nearby elliptical NGC 5128, the parent galaxy to

the radio source Cen A. B97 reviews the optical properties of these two galaxies, which have similar luminosities, effective radii, velocity dispersions, minor axis dust disks and systems of shells. The present paper shows that the similarities between these two galaxies extend to their distributions of HI, which both show a warped minor-axis rotating disk that extends outward to link with HI filaments aligned with the optical shells (Schiminovich et al. 1994, see also Sparke 1996). Evidence for star formation in the shells is given in NGC 3656 by the spectral (§ 2) and color (B97) signatures, and in NGC 5128 by the detection of CO in the shells (Charmandaris et al. 2000). These strong similarities might indicate that the type of merger and the nature of the progenitors is similar for these two galaxies, providing support for the hypothesis of a spiral-spiral merger for the formation of NGC 5128 (Schiminovich et al. 1994, Schweizer 1998).

NGC 3656 may be at an earlier stage in the merger evolution, as judged by the higher asymmetry of its optical image given by the prominent southern shell. Hence we place NGC 3656 in an earlier stage than NGC 5128 in the merger age sequence of shell galaxies, and we note that the faint optical tails, HI complexes and shell colors in NGC 3656 make a useful contribution toward filling the “King gap” (Toomre 1977) between merger remnants and normal ellipticals.

We thank Francoise Combes for her fast and constructive refereeing, and M. Vogelaar for his assistance with the use of the GIPSY image processing system. This work has been supported in part by NSF grant AST-97-17177 to Columbia University. We acknowledge the use of NED and of the LEDA database, <http://leda.univ-lyon1.fr/>.

REFERENCES

- Arribas, S., Carter, D., Cavaller, L., del Burgo, C., et al. 1998, SPIE Proceedings, 3355, 42, 821
- Balcells, M. 1997, ApJ, 486, L87 (B97)
- Balcells, M., Sancisi, R. 1996, AJ, 111, 1053 (BS96)
- Balcells, M., Stanford, S. A. 1990, ApJ, 362, 443 (BS90)
- Barnes, J. E. 2001, in Gas and Galaxy Evolution, ed. J. E. Hibbard, M. P. Rupen & J. H. van Gorkom, (San Francisco:ASP Conf Series), 240, in press
- Barnes, J. E., Hernquist, L. 1996, ApJ, 471, 115
- Bekki, K., 1998, ApJ, 499, 635
- Charmandaris, V., Combes, F., & van der Hulst, J. M. 2000, A&A, 356, L1
- Combes, F. & Charmandaris, V. 1999, ASP Conf. Ser. 182: Galaxy Dynamics - A Rutgers Symposium, 489

- del Burgo C. 2000, Ph. D. Thesis, Universidad de La Laguna.
- Dupraz, C., Combes, F. 1987, A&A, 185, L1
- Hernquist, L., Quinn, P. J. 1987, ApJ, 312, 1
- Hernquist, L., Quinn, P. J. 1989, ApJ, 342, 1
- Hernquist, L., Spergel, D. N. 1992, ApJ, 399, L117
- Hibbard, J. E., van Gorkom, J. H. 1996, AJ, 111, 655
- Hibbard, J. E., Mihos, J. C. 1995, AJ, 110, 140
- Hibbard, J. E., Vacca, W. D., & Yun, M. S. 2000, AJ, 119, 1130
- Hui, X., Ford, H. C., Freeman, K. C., Dopita, M. 1995, ApJ, 449, 592
- Jedrzejewski, R., Schechter, P. L. 1988, ApJ, 330, L87
- Kojima, M., Noguchi, M. 1997, ApJ, 481, 132
- Leitherer, ., Schaerer, D., Goldader, J. D., González-Delgado, R. M., Robert, C., Kune, D. F., de Mello, D. F., Devost, D., Heckman, T. J. 1999, ApJS, 123, 3
- Liu, C. T., Kennicutt, R. C., Jr. 1995, ApJS, 100, 325
- Mihos, J. C. 2001, ApJ, 550, 94
- Möllenhoff, C., Hummel, E., Bender, R. 1992, A&A, 255, 35
- Prieur, J. L. 1990, in "Dynamics and Interactions of Galaxies", ed. R. Wielen (Heidelberg:Springer-Verlag), 72
- Quinn, P. J. 1984, ApJ, 279, 596
- Schiminovich, D., van Gorkom, J. H., van der Hulst, J. M., Kasow, S. 1994, ApJ, 423, L101
- Schiminovich, D., van Gorkom, J. H., van der Hulst, J. M. 2001, AJ, submitted
- Schiminovich, D., van Gorkom, J. H., van der Hulst, J. M., Malin, D. F. 1995, ApJ, 444, L77
- Schweizer, F. 1996, AJ, 111, 109
- Schweizer, F. 1998, in Galaxies: Interactions and Induced Star Formation, Saas-Fee Advanced Course 26
- Sparke, L. S. 1986, MNRAS, 219, 657
- Sparke, L. S. 1996, ApJ, 473, 810

Toomre, A. 1977, in *The Evolution of Galaxies and Stellar Populations*, ed. B. M. Tinsley & R. B. Larson, (New Haven:Yale University Observatory), 401

Toomre, A., Toomre, J. 1972, *ApJ*, 178, 623

van Gorkom, J. H., Schiminovich, D. 1997, in *ASP. Conf. Ser. 116, 2d Stromlo Symp., The Nature of Elliptical Galaxies*, ed. M. Arnaboldi, G. S. da Costa, & P. Saha (San Francisco:ASP), 310

Weil, M. L., Hernquist, L. 1993, *ApJ*, 405, 1432

Zaritsky, D., Smith, R., Frenk, C., & White, S. D. M. 1997, *ApJ*, 478, 39